Absolute measurement of the Hugoniot and sound velocity of liquid copper at multimegabar pressures

Chad A. McCoy, Marcus D. Knudson, and Seth Root

Phys. Rev. B **96**, 174109 — Published 13 November 2017

DOI: 10.1103/PhysRevB.96.174109

Absolute measurement of the Hugoniot and sound velocity of liquid copper at multimegabar pressures

Chad A. McCoy[1,*], Marcus D. Knudson[1,2], and Seth Root[1]

[1]*Sandia National Laboratories, Albuquerque, NM, 87185, USA*

[2]*Institute for Shock Physics, Washington State University, Pullman, WA, 99164, USA*

**camccoy@sandia.gov*

Measurement of the Hugoniot and sound velocity provides information on the bulk modulus and Grüneisen parameter of a material at extreme conditions. The capability to launch multilayered (copper/aluminum) flyer plates at velocities in excess of 20 km/s with the Sandia Z accelerator has enabled high-precision sound velocity measurements at previously inaccesible pressures. For these experiments, the sound velocity of the copper flyer must be accurately known in the multi-Mbar regime. Here we describe the development of copper as an absolutely calibrated sound velocity standard for high-precision measurements at pressures in excess of 400 GPa. Using multilayered flyer plates, we performed absolute measurements of the Hugoniot and sound velocity of copper for pressures from 500 to 1200 GPa. These measurements enabled the determination of the Grüneisen parameter for dense liquid copper, clearly showing a density dependence above the melt transition. Combined with earlier data at lower pressures, these results constrain the sound velocity as a function of pressure enabling the use of copper as a Hugoniot and sound velocity standard for pressures up to 1200 GPa.

I. Introduction:

The high-pressure equation of state (EOS) is critical to understanding the properties of materials at conditions relevant to geophysics[1], planetary astrophysics[2, 3], ballistic and

hypervelocity impact[4, 5], and inertial confinement fusion[6]. In particular, meteoroid and debris impact for satellites in low Earth orbit can reach speeds up to 16 km/s, and EOS studies are necessary to help design debris shields able to withstand such impacts to protect the satellite. Ballistic tests to measure a material's EOS have commonly been carried out at gas gun facilities using aluminum, copper, or tantalum standards.[7-10] As a result, all three materials have been extensively characterized at the conditions accessible by single and two-stage gas guns (flyer velocities up to ~8 km/s).[7-10]

At higher pressures, EOS measurements require different drivers including three-stage hypervelocity launchers[4], explosively driven striker plates[11, 12], magnetically-launched flyer plates[13], underground nuclear explosions[14, 15], or laser-driven shocks[6, 16-18]. For these measurements to be useful, Hugoniot standards need to be extended to pressures in the thousands of GPa, and for the cases of nuclear experiments and laser-driven shocks, the off-Hugoniot behavior of standards must also be determined. For use in these cases, both the Hugoniot and off-Hugoniot response of aluminum and quartz have been constrained to pressures in excess of 1000 GPa for use as impedance matching standards in shock experiments.[19-23]

Measurement of the sound velocity in shock-compressed materials has provided information on the location of phase transitions[24-26], pressure dependence of the shear modulus[25, 26], and the Grüneisen parameter[14, 27, 28]. For pressures accessible using gas guns, absolute measurements of the sound velocity have been made using the overtaking and edge rarefaction techniques.[29] In both cases, the decrease in shock velocity or emission in an analyzer medium, such as bromoform, identifies where the overtake occurs, and the sound velocity can be determined through Lagrangian analysis.

The capability to launch layered flyer plates, fabricated through electroplating of copper onto aluminum flyers, at the Sandia Z accelerator[30] enables sound velocity measurements using the overtaking rarefaction technique at flyer velocities in excess of 20 km/s. In this type of experiment, the Hugoniot and sound velocity must be accurately known to determine the time at which the rarefaction is transmitted from the flyer into the sample of interest. While the high-pressure equation of state for copper has been extensively investigated in dynamic compression studies, [7, 10-12, 14, 15, 25, 31-35] the copper sound velocity has only been experimentally determined up to ~350 GPa;[25, 34] beyond this the sound velocity is unconstrained.

Here we present absolute measurements of the Hugoniot, sound velocity, and Grüneisen parameter of copper between 600 and 1200 GPa, enabling the use of copper flyers as an absolutely calibrated sound velocity standard for high-precision (~2-3% uncertainty) measurements at pressures in excess of 400 GPa. The measurements were made using symmetric impact of a copper-plated aluminum flyer and a copper sample. Stepped samples provided model-independent measurements of both the Hugoniot and sound velocity. For non-stepped samples a characteristics analysis was used to determine the relative sound velocity along the release from the Hugoniot state. An updated linear Hugoniot fit was calculated for pressures from 265-2000 GPa. A linear fit to the sound velocity was made in the $C_S - u_p$ plane and used to calculate the Grüneisen parameter. The results demonstrate a non-constant Grüneisen parameter in the shock-melted regime. Furthermore, the experimentaly detemined Grüneisen results do not agree with widely used EOS models for copper and provide insight into the physics governing the behavior of copper in this dense liquid regime.

II. Methods and Analysis:

Plate-impact experiments to measure the copper Hugoniot and sound velocity were conducted using the Sandia Z accelerator, a pulsed-power generator capable of generating currents in excess of 20 MA with rise times ~100-1000 ns.[30] Figure 1 shows a 2-D schematic of a typical experimental configuration using the coaxial load geometry, where a rectangular central cathode stalk is surrounded by the anode plates.[36] The north and south plates were designed to be layered copper-aluminum flyer plates with initial dimensions of approximately 40 mm in height, 20 mm in width, and 1-1.15 mm in thickness. The flyer layers were either 0.7 mm aluminum and 0.3 mm copper or 0.9 mm aluminum and 0.25 mm copper, with the copper side facing out so as to impact the samples. For three of the experiments described here, the anode box was assembled asymmetrically about the cathode stalk, with the anode-cathode gap distances (A-K gaps) being 1.4 mm and 1 mm for the north and south plates, respectively. The asymmetric construction produces different magnetic field pressures in the A-K gaps, resulting in different peak velocities for the two flyer plates. Two additional experiments had single copper samples with other samples filling the remainder of the target frame; the results of these other materials will be discussed in future publications. One experiment used the stripline geometry described in ref. 13. This stripline experiment and one of the asymmetric coaxial load experiments used thinner samples (0.3 and 0.4 mm) and enabled three Hugoniot measuements, but only one sound velocity measurement.

When firing the machine, the stored energy from the capacitor banks flows through the load generating a large magnetic field in the A-K gaps. The field interacts with the current in the flyer plates, producing a $\vec{J}\times\vec{B}$ force that drives the flyer plates outward. The flyer plates accelerate across flight gaps of 3-4 mm, depending upon peak flyer velocity, and impact the samples at velocities ranging from ~11-20 km/s, depending on the total charge voltage of the

accelerator. The current pulse is tailored to ensure that the samples are impacted by a solid density flyer which drives a steady shock into the sample.[37]

The flyer plates were fabricated by electroplating copper onto thick (~3-4 mm) diamond turned aluminum plates. After plating, the copper surface was diamond turned to the desired flyer thickness of 0.25 or 0.3 mm, and the opposing aluminum surface was diamond turned to achieve the total flyer thickness of 1 or 1.15 mm. The density of the copper layer on the flyer plate was determined using an Archimedes' balance[38] method on copper layers that had delaminated from the aluminum during the machining process. The measured density was found to be 99.3±0.2% full density (8.93 g/cm^3). Fractional thickness of the copper and aluminum was calculated from precision measurements of the flyer mass and dimensions assuming the standard density of 2.70 g/cm^3 for the aluminum and the measured copper density. The uncertainty in the thickness of the copper layer was found to be dominated by the measurement uncertainty of the lateral dimensions (~10 μm) with the measuring microscope and the variation in density of the plated copper (~2 μm). These combined uncertainties resulted in a thickness uncertainty of ~3 μm for the aluminum and copper layers. To ascertain the conditions in the flyer at impact, 1-D simulations were carried out using the magnetohydrodynamics code Laslo.[39] The simulations suggest that the pressure wave that accelerates the flyer compresses the pores in the copper and that the resultant copper layer is full density at impact with the target. The measured copper thickness was scaled to account for the full density at impact. The full density assumption is further supported by previous Hugoniot work in quartz by Knudson and Desjarlais[21] where measurements with copper plated flyers agree within uncertainty to those with solid aluminum flyers.

Two experiments (Z2186 and Z2187) used stepped copper samples, nominally 40 mm in height and 10 mm in width, with thicknesses of 0.7, 0.9, 1.1, and 1.3 mm. Step heights were measured using a through-the-lens laser auto focus instrument, with thickness precision of ~1 μm. Quartz windows, nominally 4.5 mm square and 1.5 mm thick, were mounted to each step of the copper samples using a low viscosity epoxy (Angstrombond). The stepped samples were tacked into the target frame using a UV-cured epoxy around the edges of the sample. α-quartz windows with antireflective coatings (@ 532 nm) on both sides were similarly mounted above and below the stepped copper sample.

Two experiments (Z3011 and Z3029) used single copper samples, nominally 4 mm square, with thickness of ~0.7 mm. These samples were backed by quartz windows 5 mm square with thickness of approximately 1.5 mm.

A multi-point velocity interferometer system for any reflector (VISAR)[40] was used to measure both the flyer velocity and the shock velocity within the quartz windows (the shock front in the quartz was reasonably reflective in the visible spectrum). The VISAR probe is a frequency doubled Nd:YAG laser operating at 532 nm. Because quartz is largely transparent to 532 nm light, the VISAR probe reflected directly off the copper layer of the Cu/Al flyer, accurately tracking its velocity from rest to impact. Ambiguity in fringe shift upon impact of the quartz window or shock breakout from copper into quartz was mitigated through the use of three different VISAR sensitivities, or velocity per fringe (VPF) settings, at each measurement location. The highest sensitivity VPF used in these experiments was nominally 0.277 km/s/fringe, with the exact VPF value measured after each experiment. The uncertainty in the VISAR measurements is conservatively estimated at one-tenth of a fringe, resulting in flyer plate and quartz shock velocity uncertainties of a few tenths of one percent.

II. a) Absolute Hugoniot determination:

The copper shock velocity was determined from the transit time for the shock to traverse the copper sample. For stepped samples, the flyer velocity and impact time were measured at the top and bottom of the sample; linear interpolation was then used to determine impact time and shock velocity for each step. These values differed by <0.2 ns in impact time and <0.01 km/s in flyer velocity across the sample. The transit time was averaged over the two thinnest copper steps; in these cases the subsequent shock in the quartz window exhibited some duration of a steady shock indicating that the rarefaction had not overtaken the shock front in the copper sample. For the experiments with single-thickness samples, adjacent transparent samples allowed the flyer velocity to be tracked up to impact on both sides of the copper samples; flyer velocity and impact time were similarly determined through interpolation. The uncertainties in impact and breakout time were conservatively estimated to be 0.5 ns, resulting in shock velocity uncertainties of less than 1.5%.

II. b) Absolute sound velocity determination (stepped samples):

Sound velocities were measured using the overtaking rarefaction method described originally by Al'tshuler *et al*[34]. The quartz windows mounted to the back of the copper samples were used as the analyzer material to determine the overtake time. The reflective shock front in quartz enabled use of the VISAR diagnostic to measure the shock velocity and observe the decrease in velocity at overtake, as shown in Figure 2(a). The overtake time (red star) was determined from the intersection of linear fits to both the constant-velocity plateau (black dashed) and release (pink dashed) regions. This technique is similar to previous experiments[24-26] which observed the decrease in emission of the analyzer, however it is less affected by noise and provides direct measurement of the distance into the quartz at which overtake occurs. These

advantages allow for a more precise determination of the overtake time at the shock front in the quartz and, using the quartz sound velocity, determination of the overtake time at the copper-quartz interface.

The stepped copper samples were designed such that the overtake would occur in the quartz window for the thinner steps and within the copper sample for the thicker steps. For thicker steps, where the overtake occurred within the copper sample, the constant velocity plateau fits from the previous steps were averaged. The release fit was extrapolated to determine the (negative) effective overtake time. The thickness, d_C, where the overtake would occur at the copper-quartz interface is determined through interpolation, as shown in Figure 2(b). Once d_C has been determined, the Lagrangian sound velocity is given by,

$$C_L = \frac{d_C + d_F}{d_C - d_F} U_S , \tag{1}$$

where d_F is the thickness of the copper layer on the flyer plate, and U_S is the copper shock velocity. The linear fits to the plateau and release were performed by solving the Vandermonde matrix[41] for each region using a weighted Monte Carlo technique[42] where the range of time over which the fits were computed varied from 5-15 ns on either side of the estimated overtake time. Initial weights were set as the uncertainty in the VISAR measurement (~10% of a fringe) at all times along the shock profile. The mean and standard deviation of the overtake time was calculated from 10^4 independent runs for each target step. This allowed for the overtake time to be inferred to better than 1 ns.

II.c) Relative sound velocity determination (single thickness samples):

Figure 3 illustrates the application of the overtaking rarefaction method for the single thickness samples. In this case, the overtake occurs in the quartz window backing the copper

sample, thus the inferred sound velocity for copper at the Hugoniot state depends on the sound velocities of both quartz (green dashed line) and partially released copper (orange dotted line). The quartz sound velocity was calculated from the slope the quartz release curves defined in the release model by Knudson and Desjarlais.[22] The sound velocity of the partially released copper, C_L^{rel}, can be approximated from the individual overtake times for the thinner steps of the stepped copper targets discussed above. At each of these thinner steps, the sound velocity at the Hugoniot state, C_L, is known from equation 1. The overtake time at the quartz-copper interface, t_C, is determined by integrating the quartz shock velocity from t_C to the overtake time within the quartz (which provides the distance into the quartz where the rarefaction overtook the shock front) and dividing that distance by the quartz sound velocity. C_L^{rel} is then found by solving the system of 3 equations which describe the post-shock characteristics (blue dashed and orange dotted lines) in Figure 3:

$$t_i = \frac{t_l + t_B}{2} + \frac{d_T + d_F}{2C_L}, \tag{2}$$

$$x_i = C_L\left(t_i - t_l\right), \text{ and} \tag{3}$$

$$C_L^{rel} = \frac{x_i - \left(d_T + d_F\right)}{t_i - t_C}, \tag{4}$$

where $\left(x_i, t_i\right)$ are the coordinates of the intersection of the characteristics in Figure 3, $t_l = \frac{d_F}{U_S}$ is the time at which the rarefaction wave is launched, t_B is the time at which the shock breaks out from the copper into the quartz, and d_T is the thickness of the target.

A scale factor for the partially released copper sound velocity, defined as $S_{C_L} = \frac{C_L^{rel}}{C_L} = 0.85 \pm 0.11$, was obtained by averaging the scale factors determined for the thin steps of the stepped copper targets (used for the absolute sound velocity determination described in Section II.b), where the overtake occurred in the quartz. No pressure dependence was observed for S_{C_L} across the four stepped copper experiments; comparison with the SESAME 3325[39] EOS table also demonstrated a constant relationship between C_L and C_L^{rel}. For the single thickness copper samples, equations 2-4 were then solved with C_L^{rel} replaced by $S_{C_L} C_L$. The uncertainty in S_{C_L} contributed ~1% to the uncertainty in the sound velocity at the 1σ level, less than the contribution due to the uncertainties in both thickness and timing.

III. Results and Discussion:

III.a) Absolute Hugoniot:

These absolute $U_S - u_p$ Hugoniot measurements, listed in Table I and shown in Fig. 4, double the number of absolute Hugoniot data for copper over the range of particle velocities from 5.7 to 8.2 km/s (~620-1130 GPa). Over this presssue range, these results are in good agreement with previous absolute measurements by Glushak *et al*[11] and Kormer *et al*[12], as well as corrected nuclear impedance match measurements by Mitchell *et al*[14]. The three points with uncertainties in shock velocity greater than 0.2 km/s were obtained from experiments using thin samples. For the remainder of the points, the uncertainties are smaller than those of previous data in this pressure range, which helps to further constrain the $U_s - u_p$ relationship.

A weighted, least-squares linear fit was performed using the present results and previous data for shock melted copper up to 2000 GPa. The fit and covariance matrix, calculated using a Monte Carlo technique to generate 10^6 analytic linear fits with weightings as described in Ref. 3,

are given in Table II. To determine the range of validity, we considered both the high pressure fit (>500 GPa), as performed by Kalitkin *et al*[43], and the break point between high and low pressure branches at $u_p = 4.27$ km/s, per Knudson and Desjarlais.[22] We found the fit coefficients to be rather insensitive to the u_p lower bound, and thus chose our fit to include all data above ~265 GPa, which corresponds to the completion of melt along the Hugoniot.[25]

This $U_S - u_p$ fit was compared to previous fits performed by Kalitkin *et al*[43], Trunin *et al*[44], Knudson and Desjarlais[22], and McQueen *et al*[45]. For u_p less than 10 km/s, the present fit better represents the data. Specifically, the fits by Kalitkin *et al* and McQueen *et al* significantly overpredict the slope of $U_S - u_p$, and fall outside the uncertainty of more than half the experimental data for particle velocities above 5 km/s. Trunin *et al* used a quadratic form rather than the linear $U_S - u_p$ relation used by others. Their fit agrees well with data below 5 km/s and above 10 km/s, but is systematically low in the intermediate particle velocity range. This is reasonable as the fit was constrained primarily by low pressure explosive-driven and high pressure nuclear-driven data. The fit by Knudson and Desjarlais gives systematically lower shock velocities for a given u_p than the present fit, but falls within the uncertainty of both the majority of experimental results and the present fit for velocities below 10 km/s.

This Us-up fit was also compared to the SESAME 3325[39] EOS table. Both accurately represent the Hugoniot data for u_p up to 10 km/s. At higher velocities, the SESAME 3325 table better represents the curvature in the $U_S - u_p$ response identified from nuclear experiments (absent in the present fit due to the choice of a linear parameterization). The fit by Trunin *et al* also accurately captures this curvature. We note that, in this work, the linear parametrization was chosen to simplify error propagation when using the fit for impedance matching calculations.

However, by doing so, it inherently ignores the softening at ultra-high pressures identified for multiple materials[14, 15, 21, 44] and is limited in its useable pressure range. Hence, for $u_p > 10$ km/s (~1640 GPa), we recommend the use of either the SESAME 3325 model or the Trunin *et al* fit.

The difference between the various Hugoniot fits is more apparent in the $P-\rho$ plane (Figure 4(b)). The Kalitkin and McQueen fits are less compressible (stiffer) than the vast majority of data for pressures greater than 500 GPa, while the fit by Trunin is the most compressible. In contrast to Figure 4(a), where it appears to be in agreement with the data for lower pressures, the Trunin *et al* fit is outside the uncertainty of 50% of the experimental results, and hence should not be considered accurate for pressures less than 1200 GPa. The SESAME 3325 table and both our fit and that by Knudson and Desjarlais describe well the copper Hugoniot in this range.

III.b) Sound velocity:

These experiments yielded seven (four absolute and three relative) measurements of the copper sound velocity (Table I) for pressures in excess of 500 GPa, extending the measured sound velocity to 1100 GPa. Prior to this work, there were only five measurements to constrain the sound velocity for pressures in excess of the melt transition (265 GPa), with the highest pressure being less than 400 GPa. The measurements reported here are in good agreement with the previous results; extrapolation of a linear fit to only our higher pressure results in the $C_S - u_p$ plane agrees well with the earlier measurements (green circles and black squares in Figure 5). A weighted linear fit to all the sound speed measurements above melt is shown as the solid red line in Figure 5. The fit and covariance matrix parameters are given in Table III.

Over the pressure range of this study (~600-1100 GPa), the inferred slope in the $C_S - u_p$ plane is approximately 25% greater than that of either the Hayes model[25] (green dash-dot line) or

SESAME 3325 (black dashed line); the sound velocity of both models being more than 2σ lower than the majority of our results. The similarities between the Hayes and SESAME models result from the use of the measurements by Hayes and Al'tshuler to constrain the sound velocity above melt. A key feature of both models is the limited range of data used to fit the sound velocity. Because all five previous measurements covered a pressure range of only ~50 GPaextrapolation of the sound velocity to higher pressure is poorly constrained. The present results provide a much needed constraint on the behavior of copper in the ense liquid regime.

The Hayes model was developed using their experimental sound speeds with the Hugoniot of McQueen *et al* assuming both the Grüneisen parameter and the constant volume specific heat (C_V) are constant. The Hayes model shows significantly better agreement with the data when compared to the experimental results in the $C_S - \rho$ plane (Figure 6). However, this apparent agreement results from a combination of errors due to the use of the McQueen Hugoniot (which is too stiff when compared to the experimental data); the lower density compression results in an artificially high C_S and an artificially low density, both of which bring the fit into better apparent agreement with the sound velocity measurements in the $C_S - \rho$ plane.

III.c) Grüneisen parameter:

The Grüneisen parameter, Γ, for copper was determined from the present sound velocity measurements and the linear Hugoniot fit (Table II):

$$\frac{\Gamma}{2V} = \frac{\left(\frac{dP}{dV}\right)_H + \frac{C_S^2}{V^2}}{P_H + \left(\frac{dP}{dV}\right)_H (V_0 - V)}, \tag{5}$$

where $V = \frac{1}{\rho}$ is the specific volume, P_H is the Hugoniot pressure at volume V, and the derivatives are evaluated along the Hugoniot. Over the pressure range of 300-1100 GPa (corresponding to densities between 14.5 and 18.5 g/cm^3), the experimentally determined Grüneisen parameter decreases from ~1.4 to ~0.9, as shown in Figure 7. This density dependence clearly demonstrates that the assumption of a constant Grüneisen parameter made by Hayes *et al* is invalid for high-pressure liquid copper.

The trend of the present results, Γ decreasing with increasing density, is consistent with assumptions that, absent electronic and thermal contributions, $\rho\Gamma$ is constant. However, the present results decrease at a greater rate, which implies that at the (P,T) states reached in these experiments, electronic and thermal contributions have an effect on Γ. The constant Γ and C_V model assumed by Hayes does not agree with the limiting value of $\Gamma = \frac{2}{3}$ at infinite compression,[46] but was chosen because it is the simplest model that could agree with their shock data and measurements of the liquid sound velocity at ambient pressure. Furthermore, it has been shown that assuming constant Γ and C_V overpredicts the temperature along the Hugoniot,[47] implying that the temperature calculated by Hayes would be noticeably greater than in the actual experiments. Ambient measurements by Hayes[25] demonstrate that the sound velocity of liquid copper decreases with increasing temperature, hence the shocked sound velocity would be underpredicted outside the range constrained by experimental data, which is consistent with the present results.

Reanalysis of the Grüneisen parameter from the sound velocity data of Hayes using the present Hugoniot fit (Table II) decreased the inferred Grüneisen for pressures between 300 and 400 GPa from $\Gamma \approx 1.55$ to $\Gamma \approx 1.34$. This difference is entirely due to the difference in the

assumed Hugoniot response (Hayes used the McQueen fit) as both the $P-V$ state and slopes are model dependent. We also note that, over this pressure and density range, the SESAME 3325 table overestimates the Grüneisen parameter by a near constant value of ~0.11. This suggests that Hayes's data was used to constrain the Grüneisen parameter just above melt in the development of the SESAME table. Adjusting this constraint, i.e. reducing the Grüneisen parameter in the SESAME model by ~0.11, would bring the SESAME model into much better agreement with the present high pressure data. As the SESAME 3325 Hugoniot is in reasonable agreement with experiment, a systematic decrease of the Grüneisen parameter would result in a systematically higher sound velocity, in better agreement with the measured values.

The uncertainty in the inferred Grüneisen parameter is ~10%, comparable to the estimated accuracy reported by Hayes *et al*. The uncertainty is dominated by the Hugoniot slope; the covariance matrix for the present fit results in an uncertainty of ~3% in the $P-V$ derivative in equation 5. Improvement in precision would require additional Hugoniot measurements in the 300-1100 GPa range to decrease the covariance of the Hugoniot fit. Nevertheless, there is strong evidence for a density dependent Grüneisen parameter for liquid copper and that the SESAME 3325 table systematically overestimates the Grüneisen parameter in the 300-1100 GPa range.

IV. Conclusions:

The Hugoniot and sound velocity of shock-compressed copper were measured using magnetically launched flyer plates on the Sandia Z machine. Using a symmetric impact technique, absolute Hugoniot measurements were made in the pressure range of 600-1200 GPa. The results are in good agreement with previous measurements, while increasing the amount of experimental data by a factor of two. The results also agree well with the tabular SESAME 3325

EOS model. The shock and particle velocities were measured within ~1-3% and <1%, respectively, an improvement in uncertainty over all previous measurements in this range of pressures. An updated linear $U_S - u_p$ relation was determined for the liquid copper Hugoniot up to 2500 GPa.

The sound velocity of shock-compressed copper was measured for pressures in excess of 400 GPa. The results suggest a linear fit in the $C_S - u_p$ plane at high pressure is reasonable. The linear fit is consistent with the previous measurements for liquid copper, but suggests a ~25% increase in slope (with respect to u_p) compared to the widely used models. The experimentally inferred Grüneisen parameter clearly indicates a density dependence above the melt transition and provides a much needed constraint on the behavior of copper in the dense liquid regime.

The experimental fits derived in this study enable use of liquid copper as a Hugoniot and sound velocity standard. The fits demonstrate a linear dependence for both U_S and C_S with respect to u_p is adequate for shock melted copper up to 1200 GPa. Considering the curvature of the Hugoniot, it is likely that these fits could be reasonably extrapolated up to ~1600 GPa, however caution should be used at higher pressures due to possible softening of the Hugoniot response relative to our linear fits due to ionization. The inferred Grüneisen response allows for the use of a Mie-Grüneisen EOS with our linear Hugoniot fit to determine the re-shock or release of liquid copper for impedance matching measurements.

Acknowledgements:

We would like to thank the teams at Sandia that assisted with target design and fabrication as well as the experimental team that fielded the VISAR diagnostics and operated the *Z* facility. Sandia National Laboratories is a multimission laboratory managed and operated by National Technology and Engineering Solutions of Sandia, LLC., a wholly owned subsidiary of

Honeywell International, Inc., for the U.S. Department of Energy's National Nuclear Security Administration under contract DE-NA0003525.

References:

1. F. Coppari, R. F. Smith, J. H. Eggert, J. Wang, J. R. Rygg, A. Lazicki, J. A. Hawreliak, G. W. Collins and T. S. Duffy, Nat. Geo. **6** (11), 926-929 (2013).

2. M. D. Knudson, M. P. Desjarlais and D. H. Dolan, Science **322** (5909), 1822–1825 (2008).

3. S. Root, L. Shulenburger, R. W. Lemke, D. H. Dolan, T. R. Mattsson and M. P. Desjarlais, Phys. Rev. Lett. **115** (19), 198501 (2015).

4. L. C. Chhabildas, L. N. Kmetyk, W. D. Reinhart and C. A. Hall, Int. J. Imp. Engin. **17** (1–3), 183-194 (1995).

5. E. A. Taylor, J. P. Glanville, R. A. Clegg and R. G. Turner, Int. J. Imp. Engin. **29** (1), 691-702 (2003).

6. M. A. Barrios, T. R. Boehly, D. G. Hicks, D. E. Fratanduono, J. H. Eggert, G. W. Collins and D. D. Meyerhofer, J. Appl. Phys. **111** (9), 093515 (2012).

7. A. C. Mitchell and W. J. Nellis, J. Appl. Phys. **52** (5), 3363–3374 (1981).

8. N. C. Holmes, J. A. Moriarty, G. R. Gathers and W. J. Nellis, J. Appl. Phys. **66** (7), 2962-2967 (1989).

9. W. J. Nellis, A. C. Mitchell and D. A. Young, J. Appl. Phys. **93** (1), 304-310 (2003).

10. W. M. Isbell, F. H. Shipman and A. H. Jones, *Hugoniot equation of state measurements for eleven materials to five megabars*, General Motors Corp., Material Science Laboratory Report MSL-68–13, 1968.

11. B. L. Glushak, A. P. Zharkov, M. V. Zhernokletov, V. Ya. Ternovoi, A. S. Filimonov and V. E. Fortov, Zh. Eksp. Teor. Fiz **96**, 1301 (1989).

12. S. B. Kormer, A. I. Funtikov, V. D. Urlin and A. N. Kolesnikova, Sov. Phys. J. Expt. Theor. Phys. **15** (3), 477-488 (1962).

13. R. W. Lemke, M. D. Knudson and J.-P. Davis, Int. J. Imp. Engin. **38** (6), 480-485 (2011).

14. A. C. Mitchell, W. J. Nellis, J. A. Moriarty, R. A. Heinle, N. C. Holmes, R. E. Tipton and G. W. Repp, J. Appl. Phys. **69** (5), 2981-2986 (1991).

15. R. F. Trunin, Physics-Uspekhi **37** (11), 1123-1145 (1994).

16. C. A. McCoy, M. C. Gregor, D. N. Polsin, D. E. Fratanduono, P. M. Celliers, T. R. Boehly and D. D. Meyerhofer, J. Appl. Phys. **119** (21), 215901 (2016).

17. P. M. Celliers, G. W. Collins, L. B. Da Silva, D. M. Gold and R. Cauble, Appl. Phys. Lett. **73** (10), 1320–1322 (1998).

18. R. Cauble, T. S. Perry, D. R. Bach, K. S. Budil, B. A. Hammel, G. W. Collins, D. M. Gold, J. Dunn, P. Celliers, L. B. Da Silva, M. E. Foord, R. J. Wallace, R. E. Stewart and N. C. Woolsey, Phys. Rev. Lett. **80** (6), 1248–1251 (1998).

19. T. R. Boehly, J. E. Miller, D. D. Meyerhofer, J. G. Eggert, P. M. Celliers, D. G. Hicks and G. W. Collins, AIP Conf. Proc. 955, 19–22 (2007).

20. D. G. Hicks, T. R. Boehly, P. M. Celliers, J. H. Eggert, E. Vianello, D. D. Meyerhofer and G. W. Collins, Phys. Plasmas **12**, 082702 (2005).

21. M. D. Knudson and M. P. Desjarlais, Phys. Rev. Lett. **103** (22), 225501 (2009).

22. M. D. Knudson and M. P. Desjarlais, Phys. Rev. B **88** (18), 184107 (2013).

23. M. D. Knudson, M. P. Desjarlais and A. Pribram-Jones, Phys. Rev. B **91** (22), 224105 (2015).

24. J. H. Nguyen and N. C. Holmes, Nature **427** (6972), 339-342 (2004).

25. D. Hayes, R. S. Hixson, R. G. McQueen, M. D. Furnish, L. C. Chhabildas and R. S. Hixson, AIP Conf. Proc. **505** (1), 483-488 (2000).

26. J. H. Nguyen, M. C. Akin, R. Chau, D. E. Fratanduono, W. P. Ambrose, O. V. Fat'yanov, P. D. Asimow and N. C. Holmes, Phys. Rev. B **89** (17), 174109 (2014).

27. D. E. Fratanduono, P. M. Celliers, D. G. Braun, P. A. Sterne, S. Hamel, A. Shamp, E. Zurek, K. J. Wu, A. E. Lazicki, M. Millot, and G. W. Collins, Phys. Rev. B **94** (18), 184107 (2016).

28. C. A. McCoy, M. C. Gregor, D. N. Polsin, D. E. Fratanduono, P. M. Celliers, T. R. Boehly and D. D. Meyerhofer, J. Appl. Phys. **120** (23), 235901 (2016).

29. Ya. B. Zel'dovich and Yu. P. Raizer, *Physics of Shock Waves and High-Temperature Hydrodynamic Phenomena*. (Dover Publications, 2002).

30. M. E. Savage, L. F. Bennett, D. E. Bliss, W. T. Clark, R. S. Coats, J. M. Elizondo, K. R. LeChien, H. C. Harjes, J. M. Lehr and J. E. Maenchen, Pulsed Power Conference, 2007 16th IEEE International **2**, 979-984 (2007).

31. L. V. Al'Tshuler, A. A. Bakanova and R. F. Trunin, Sov. Phys. J. Expt. Theor. Phys. **15** (6) (1962).

32. M. Yokoo, N. Kawai, K. G. Nakamura and K. Kondo, Int. J. Imp. Engin. **35** (12), 1878-1883 (2008).

33. L. V. Al’tshuler, S. B. Kormer, A. A. Bakanova and R. F. Trunin, Sov. Phys. J. Expt. Theor. Phys. **11** (3), 573–579 (1960).

34. L. V. Al'Tshuler, S. B. Kormer, M. I. Brazhnik, L. A. Vladimirov, M. P. Speranskaya and A. I. Funtikov, Sov. Phys. J. Expt. Theor. Phys. **11** (4), 766 (1960).

35. R. G. Kraus, J.-P. Davis, C. T. Seagle, D. E. Fratanduono, D. C. Swift, J. L. Brown and J. H. Eggert, Phys. Rev. B **93** (13), 134105 (2016).

36. M. D. Knudson, R. Lemke, D. Hayes, C. A. Hall, C. Deeney and J. Asay, J. Appl. Phys. **94** (7), 4420-4431 (2003).

37. R. W. Lemke, M. D. Knudson, D. E. Bliss, K. Cochrane, J.-P. Davis, A. A. Giunta, H. C. Harjes and S. A. Slutz, J. Appl. Phys. **98** (7), 073530 (2005).

38. S. W. Hughes, Phys. Educ. **40** (5), 468 (2005).

39. J. H. Carpenter, *private communication* (2016).

40. L. M. Barker and R. E. Hollenbach, J. Appl. Phys. **43** (11), 4669–4675 (1972).

41. G. H. Golub and C. F. V. Loan, *Matrix computations (3rd ed.)*. (Johns Hopkins University Press, 1996).

42. P. W. Holland and R. E. Welsch, Commun. Stat. Theory Methods **6** (9), 813-827 (1977).

43. N. N. Kalitkin and L. V. Kuz'mina, Physics-Doklady **44**, 589-591 (1999).

44. R. F. Trunin, *Experimental Data on Shock Compression and Adiabatic Expansion of Condensed Matter* (Russian Federal Nuclear Center-VNIIEF, Sarov, 2001).

45. R. G. McQueen, S. P. Marsh, J. W. Taylor, J. N. Fritz and W. J. Carter, in *High-Velocity Impact Phenomena*, edited by R. Kinslow (Academic Press, New York, 1970), pp. 293–417.

46. S. B. Segletes and W. P. Walters, J. Phys. Chem. Solids **59** (3), 425-433 (1998).

47. C. D. Yarrington, D. Kittell, R. R. Wixom and D. L. Damm, J. Phys. Conf. Ser. **500** (5), 052053 (2014).

Table I: Hugoniot and sound velocity measurements for liquid copper on the Sandia Z machine. Shots Z2112 and Z2241 used thin samples and hence have greater uncertainty in the Hugoniot state. Sound velocity measurements were not obtained for Z2112 or Z2241S. The Grüneisen parameter, Γ, was calculated using the Hugoniot fit given in Table II.

Shot	v_F (km/s)	u_p (km/s)	U_S (km/s)	P (GPa)	ρ (g/cm^3)	C_S (km/s)	Γ
Z2112	16.27±0.05	8.14±0.05	15.57±0.26	1132.0±19.4	18.73±0.35	--	--
Z2186N	11.42±0.03	5.71±0.03	12.22±0.09	622.9±5.5	16.76±0.13	11.57±0.18	1.11±0.09
Z2186S	12.48±0.03	6.24±0.03	13.41±0.11	747.3±6.7	16.71±0.13	12.30±0.23	0.86±0.12
Z2187N	14.47±0.03	7.24±0.03	14.41±0.12	932.5±8.7	17.95±0.17	13.66±0.25	0.98±0.10
Z2187S	15.64±0.03	7.82±0.03	15.40±0.14	1075.0±10.6	18.14±0.18	14.29±0.29	0.91±0.12
Z2241N	13.73±0.10	6.87±0.10	14.10±0.25	865.0±19.9	17.42±0.38	13.40±1.07	0.85±0.33
Z2241S	14.72±0.08	7.36±0.08	15.05±0.25	988.5±19.7	17.47±0.33	--	--
Z3011	15.25±0.04	7.63±0.04	15.19±0.19	1035.3±13.9	17.95±0.24	13.97±0.36	0.92±0.13
Z3029	12.20±0.03	6.10±0.03	12.95±0.16	706.2±9.3	16.89±0.19	12.01±0.32	1.03±0.13

Table II: Fit and covariance matrix parameters for liquid copper Hugoniot ($U_S = C_0 + Su_p$).

C_0 (km/s)	S	$\sigma^2_{C_0}$ ($\times 10^{-3}$)	σ^2_S ($\times 10^{-4}$)	$\sigma_{C_0}\sigma_S$ ($\times 10^{-3}$)
4.272	1.413	5.964	2.315	-1.116

Table III: Fit and covariance matrix parameters for liquid copper Eulerian sound velocity ($C_S = a + bu_p$).

a (km/s)	b	σ^2_a ($\times 10^{-2}$)	σ^2_b ($\times 10^{-3}$)	$\sigma_a\sigma_b$ ($\times 10^{-2}$)
4.076	1.311	6.918	2.364	-1.232

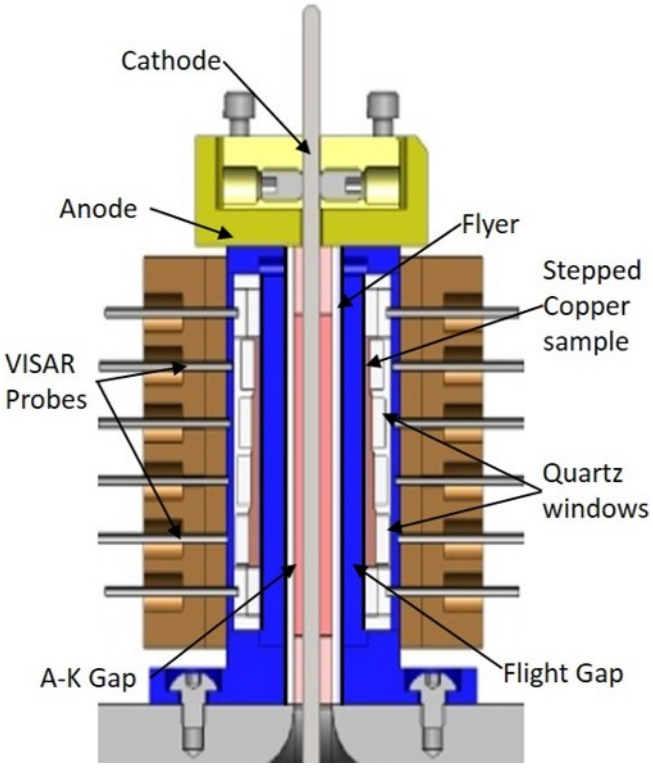

Figure 1: (Color online) Cutout view of the coaxial load geometry used for all shots except Z2112 (which used the stripline geometry), illustrating target assembly and probe mounting for VISAR diagnostic. Stepped copper targets were used on Z2186 and Z2187 with individual samples mounted in the target frame for the remaining shots.

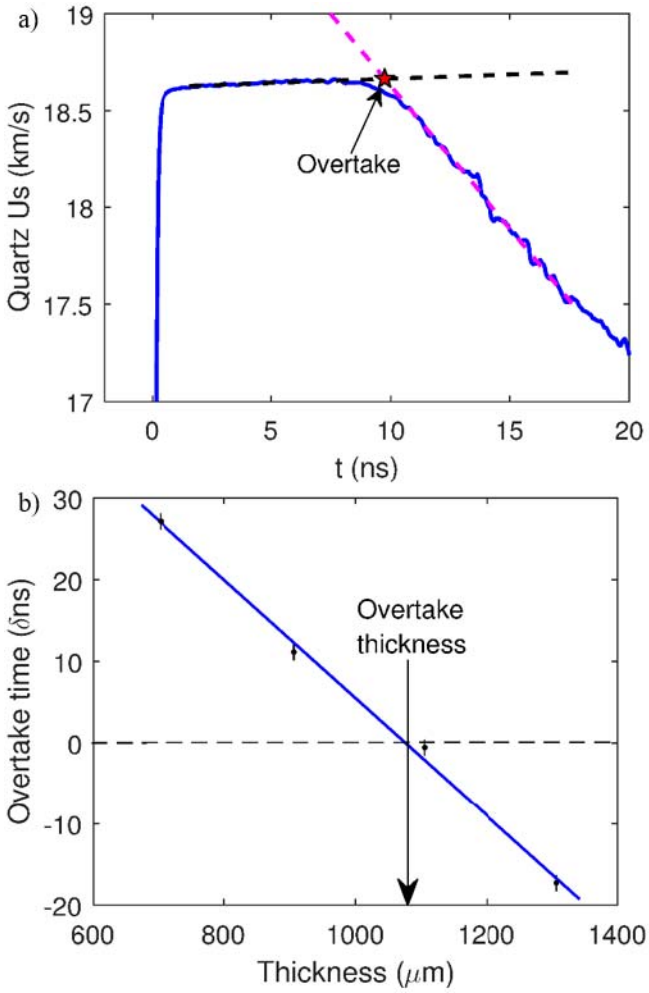

Figure 2: (color online) (a) Typical overtake measurement in the quartz window. The shock velocity in the quartz (blue solid) provides a precise measurement of the overtake time through the sudden decrease in shock velocity upon overtake by the rarefaction wave. The constant plateau (black dashed) and release (pink dashed) are linearly fit and extrapolated to determine the overtake time (red star). (b) Overtake time as a function of step thickness. The thickness at which overtake occurs at the copper-quartz interface is determined by $\delta t = 0$ and noted with the black arrow.

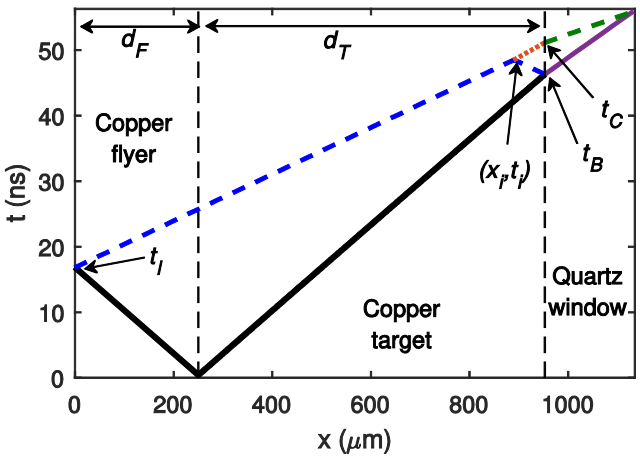

Figure 3: (color online) $x-t$ diagram showing rarefaction waves (dashed lines) overtaking a shock (solid lines) in the Lagrangian frame of a target. For the stepped target, the sound velocity in the shocked copper (blue dashed) is determined from the overtake thickness at the interface (Figure 2(b)). This velocity is used with the overtake time at the interface determined from the shock (purple solid) and rarefaction (green dashed) in the quartz to determine the rarefaction wave speed in the released copper (orange dotted).

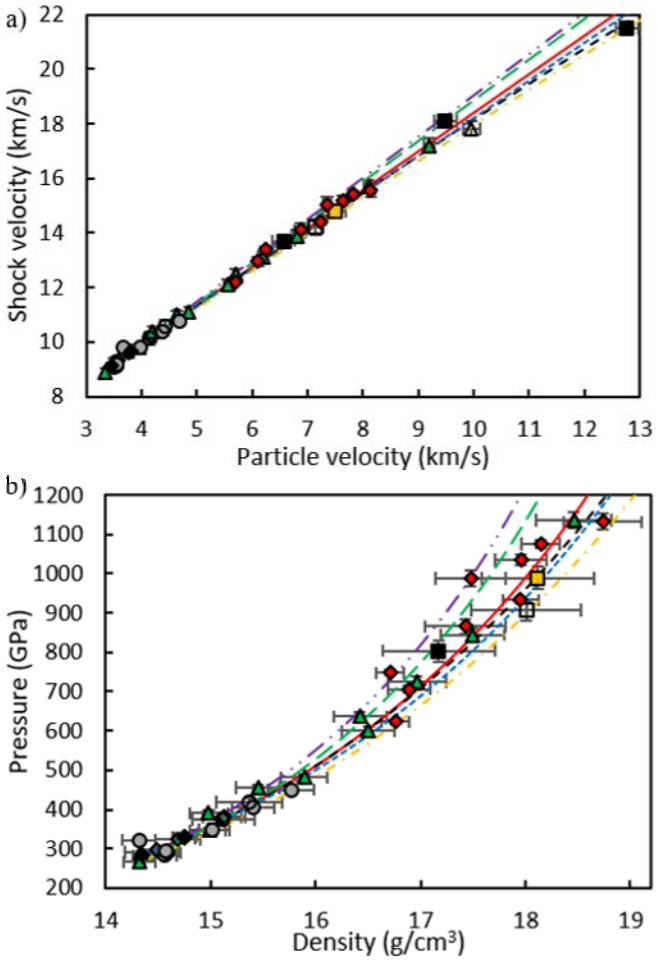

Figure 4: (color online) (a) $U_S - u_p$ plot showing Hugoniot measurements in this work (red diamonds) as well as previous measurements from Ref. [33] (open circles), Ref. [31] (open squares), Ref. [12] (orange squares), Ref. [10] (gray circles), Ref. 7 (black diamonds), Ref. [11] (green triangles), Ref. [14] (black squares), Ref. [15] (open triangles), and Ref. [32] (open diamonds). Fits from this work (red solid), Kalitkin[43] (purple dash-dot-dot), McQueen[45] (green long dash), Trunin[44] (orange dash-dot), Knudson[22] (blue dot), and SESAME 3325[39] (black dash) are also shown. (b) $P - \rho$ Hugoniot illustrating the present linear fit, the Knudson linear fit, and the SESAME 3325 table exhibit the best agreement with experimental the data; both Kalitkin and McQueen are noticeably less compressible (stiffer) and Trunin is more compressible (softer).

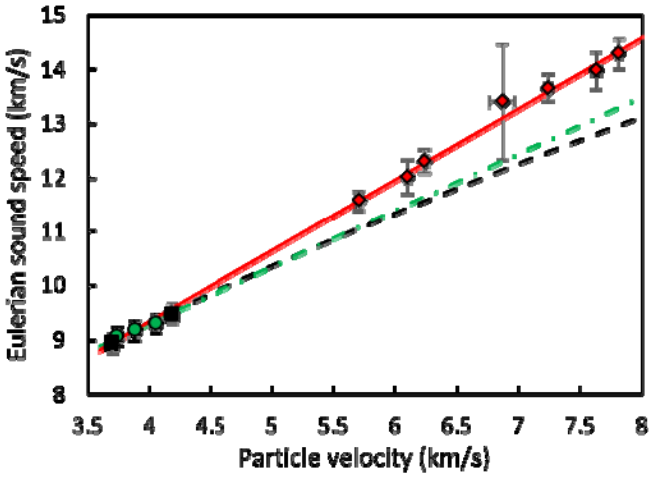

Figure 5: (color online) Eulerian sound velocity as a function of particle velocity, A linear fit (red solid) to the present data (red diamonds) is in excellent agreement with the data of Al'tshuler[34] (black squares) and Hayes[25] (green circles). The slope of the present fit is noticeably steeper than that of the Hayes (green dash-dot) and SESAME 3325 (black dash) models.

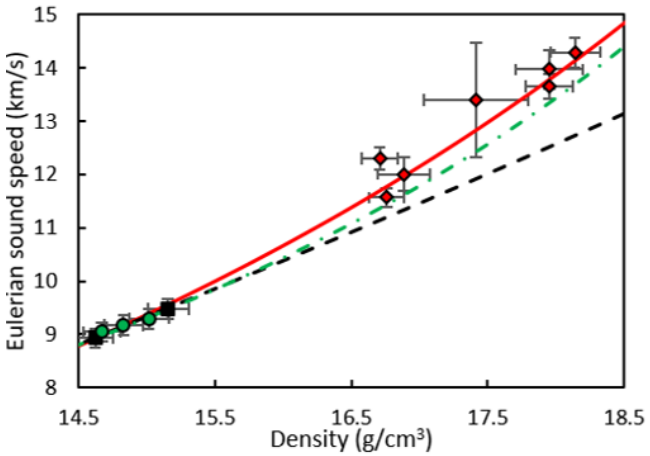

Figure 6: (color online, lines and symbols same as Figure 5) Eulerian sound velocity as a function of density. The Hayes model appears to be in better agreement with the experimental results when viewed in this plane, however, this results from a combination of errors due to the use of the McQueen Hugoniot fit to infer sound speed from their data.

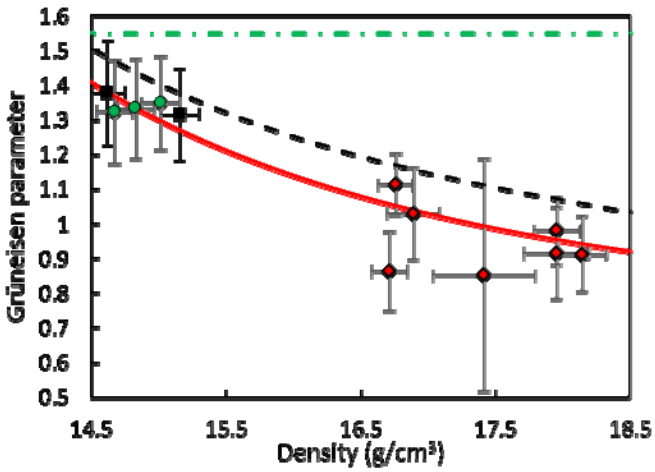

Figure 7: (color online, lines and symbols same as Figure 5) The Grüneisen parameter as a function of density. The present work shows a distinct density dependence for liquid copper. The SESAME 3325 table also exhibits similar density dependence, however the Grüneisen parameter is systematically ~0.11 larger. In constrast, Hayes assumed a constant Grüneisen parameter of 1.55 for liquid copper.